External cavity terahertz quantum cascade laser with a metamaterial/graphene optoelectronic mirror.

Nikita W. Almond,[1] Xiaoqiong Qi,[2] Riccardo Degl'Innocenti,[3,a] Stephen J. Kindness,[1] Wladislaw Michailow,[1] Binbin Wei,[1] Philipp Braeuninger-Weimer,[4] Stephan Hofmann,[6] Paul Dean,[5] Dragan Indjin,[5] Edmund H. Linfield,[5] A. Giles Davies,[5] Aleksandar D. Rakić,[2] Harvey E. Beere,[1] David A. Ritchie[1]

[1]Cavendish Laboratory, University of Cambridge, J. J. Thomson Avenue, Cambridge CB3 0HE, UK
[2]School of Information Technology and Electrical Engineering, the University of Queensland, Brisbane, QLD 4072 Australia
[3]Department of Engineering, Lancaster University, Lancaster, LA1 4YW, UK
[4]Department of Engineering, University of Cambridge, 9 J J Thomson Avenue, Cambridge, CB3 0FA, UK
[5]School of Electronic and Electrical Engineering, University of Leeds, Leeds, LS2 9JT, United Kingdom

[a]E-mail: r.deglinnocenti@lancaster.ac.uk

Abstract

Photonic engineering of the terahertz emission from a quantum cascade laser (QCL) is fundamental for the exploitation of this unique source in a myriad of applications where it can be implemented, such as spectroscopy, imaging and sensing. Active control of the frequency, power, polarization and beam profile has been achieved through a variety of approaches. In particular, the active control of the emitted frequency, which is difficult to determine *a priori*, has been achieved through the integration of a photonic structure, and/or by using external cavity arrangements. In this work an external cavity arrangement which implements a metamaterial/graphene optoelectronic mirror as external feedback element is proposed and demonstrated. The reflectivity and dispersion properties of the external active mirror were tuned via electrostatically gating graphene. It was possible to electronically reproduce the mode-switch occurring in a QCL emitting ~ 2.8 THz by mechanically changing the external cavity length formed by an Au mirror. The external cavity arrangement was investigated and described in the framework of self-mixing theory. These results open a way for all-electronic engineering of the QCL emission by the use of a fast reconfigurable external mirror. This approach can uniquely address both power and frequency control, with ~ 100 MHz reconfiguration speeds, using an integrated external element. Furthermore, the

metamaterial/graphene mirror strong dispersive properties might be implemented for active mode locking of THz QCLs. Finally, this approach offers a unique opportunity to study the laser dynamics and mode competition in THz QCLs in the self-mixing feedback regime.

High power [1], and recently thermoelectrically cooled [2] terahertz quantum cascade lasers (THz-QCLs) have opened up areas of research in a myriad of applications such as spectroscopy [3, 4], imaging [5-7] and potentially communications [8]. In particular, the engineering of the photonic emission properties [9], frequency [10-13], polarization [14] and beam profile [15-16] has been exploited in multiple configurations. Direct modulation of the driving current yields a frequency shift on the order of ~ 10 GHz through exploiting the Stark effect, but not all the quantum designs are equally suitable for this approach, nor can the exact frequency be determined a priori by cleaving standard ridges. Continuous frequency modulation has been demonstrated over a > 100 GHz range, with a plethora of external cavity arrangements [17-19]. Several configurations have been demonstrated as effective in achieving a large modulation span, but either require a complex fabrication and/or the implementation of a nano-positioning controller inside the cryostat, or are intrinsically slow, due to the reliance on thermal effects [20] and mechanical tunable elements [21]. Different from the direct modulation of the laser driving bias, our approach provides a fast electronic and fully independent method to control the QCL emission. Lately metamaterials [22, 23], subwavelength artificial atoms, have started to be integrated with QCLs thanks to their high efficiency, adaptability and a priori engineered frequency response. An interesting approach has recently emerged [15, 16] in which metamaterial arrays loaded with an active material have been combined with an external cavity. Alternatively, metamaterial arrays loaded with graphene, providing the active element, have been demonstrated as a versatile tool for the realization of fast reconfigurable THz active devices, such as in amplitude [24, 25], frequency [26] and polarization [27, 28] modulators. Metamaterial/graphene amplitude modulators have been used as a tunable external cavity mirror [29] in combination with quantum cascade amplifiers [30], and also for active amplitude stabilization [31]. Through this approach, by

2

electronically modulating the reflectance of the external metamaterial mirror, lasing action could be switched on as well as the emitted optical modes selectively enhanced or suppressed. In this manuscript, two different QCL external cavity arrangements have been investigated and compared in a proof of principle experiment. The first one implemented a standard Au mirror as an external reflector in combination with a partially suppressed QCL. By sweeping the position of the mirror, the power and spectral contents of the laser emission were tuned. The results obtained were perfectly reproduced by substituting the Au mirror with a fixed optoelectronic reconfigurable mirror with electrically tunable reflectance. The optoelectronic device consists of a metamaterial array loaded with monolayer graphene patches, capable of dynamically changing its dispersive properties by varying the graphene conductivity. The metamaterial array was designed in order to provide a more dispersive reflectance compared to Ref. [29] and hence improved frequency selectivity. The two systems were thoroughly investigated and modeled using multi-mode reduced rate equations (RREs) model fed by the full self-consistent energy-balance Schrödinger–Poisson electron transport QCL solver [32, 33] in order to gain further insight into the mode tuning characteristics. These results pave the way to the realization of all-electronic fast reconfigurable external modulation of the QCL emission. This approach is compatible with all QCL designs and cavities, does not require any photonic patterning or moving elements, and introduces a further independent degree of freedom to act on the laser emission. Further to this, the high-speed and dispersion flexibility offered by this approach could be exploited in spectroscopy, for active beam focusing devices, or even for the realization of QCL active mode-locking [34].

The experimental arrangement of the external cavity QCL (EC-QCL) measurements is showed in Figure 1. The QCL was fabricated from a bound-to-continuum design with a central frequency ~2.8 THz into a 2.5 mm-long single-plasmon ridge. A 2.67 mm-diameter hemispherical Si-lens coated with 18.5 μm-thick layer of parylene-C (n_{par}= 1.62, absorption coefficient = 27 cm^{-1}) was attached with Poly-methyl methacrylate (PMMA) to one facet of the QCL to suppress/reduce the lasing emission, by reduction of the reflectivity of that facet, and also to improve collimation. The QCL was mounted on the cold-finger of a continuous flow

liquid helium cryostat with a THz transparent high density polyethylene tube used as the outer shroud. The laser was typically operated in pulsed mode with a 10 kHz repetition rate, 10% duty cycle and ~300 Hz gating frequency. The radiation emitted from the QCL facet without the lens was collimated into a fast Fourier Transform Infrared (FTIR) spectrometer from Bruker (model IFS 66 v/S, 0.25 cm^{-1} resolution). The emitted power and the spectra were acquired using a Si-Ge 4 K bolometer. The signal demodulation and acquisition were performed with a lock-in amplifier using the gating frequency as the reference and the output of the bolometer as input. The THz radiation emitted from the coated-lens facet side was collimated and focused
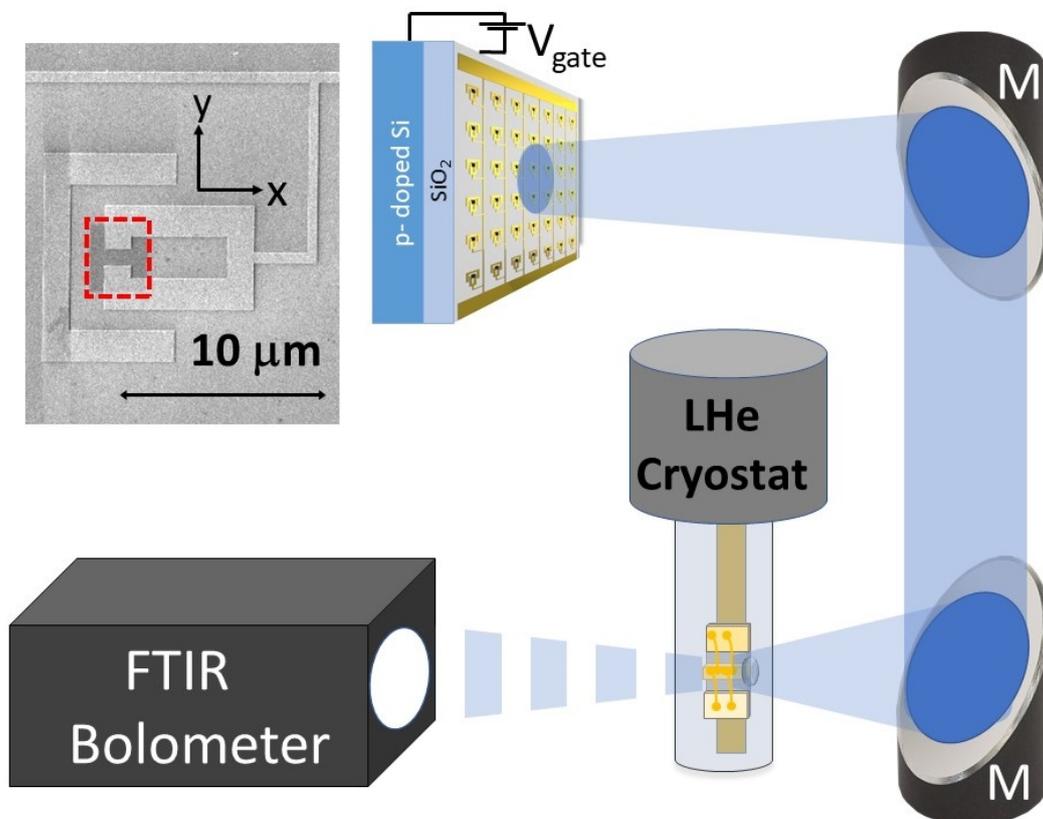

Figure 1; Schematic of the experimental arrangement implemented for the EC-QCL measurements with a metamaterial/graphene external reflecting target. The EIT mirror position was kept fixed and the spectra recorded for different graphene gate voltages V_{gate}. The inset shows a single EIT unit, where the red dashed line denote the graphene patch shunting the inner ring.

onto the feedback element with two parabolic mirrors with a focal length of 5 cm and 7 cm respectively. The external mirror was placed at a distance of approximately 14 cm from the Si-lens facet. The external mirrors used in these measurements were either a standard Au mirror or a metamaterial/graphene optoelectronic device. The metamaterial/graphene device is similar to the first device characterized in Ref. [26] but with dimensions scaled by a factor 0.48

in order to match the QCL frequency range. The unit cell, shown in Figure 1, is based on two coupled resonators having a similar resonant frequency and it exhibits an inherently dispersive electromagnetically induced transparency (EIT) analogue. The larger C-shaped resonator (7.5x10 μm^2) strongly interacts with the incident field parallel to the longest side. The inner ring supports a dark mode, which is indirectly excited by strong capacitive coupling with the outer resonator, and is shunted by a graphene patch. Active damping of the dark resonator achieved through electrostatic modulation of the graphene conductivity, modifies the coupling between these two modes and the overall optical response. The device consists of a 1x1 mm^2 array of identical metallic (Ti/Au 10/80 nm) resonators defined by electron beam lithography, thermal evaporation and lift-off on a p-doped Si/SiO$_2$ (500 μm/ 300 nm) chip. Chemical vapour deposition grown graphene [35] was transferred on top of the array and patterned into patches, by further e-beam lithography and plasma etching, shorting the smaller resonators, as showed in Figure 1. Biasing metallic lines were added in order to allow electrostatic gating of the graphene, after which the device was wire bonded and packaged. The graphene conductivity range and the Dirac point were experimentally measured from a uniform graphene control area, fabricated together with the metamaterial device. The resistance between source and drain pads on this area has been recorded for different back gate voltages by using two source/meter units (Keithley, 2400 model) to retrieve the Dirac point and infer the accessible conductivity range [26]. As the electrostatic gating of the device was varied between 60 V (Dirac point) and -100 V, the graphene conductivity was swept between 0.6 mS and 1.4 mS, respectively. The graphene conductivity acquired at different back-gate voltages is reported in the Supplementary Information (SI). In the first set of experiments instead of the EIT optoelectronic device, a planar highly reflective gold mirror positioned on a linear micrometer motorized stage was used as the feedback element.

The complex refractive index and reflectivity of the EIT mirror for different graphene conductivities was calculated with the finite element method (FEM) based Comsol Multiphysics V5.3a software. A single unit cell was used in these simulations having lateral Floquet boundary conditions to simulate a continuous metamaterial array. The incoming THz radiation

was simulated using a top port emitting with the E-field polarization along the longer axis of the
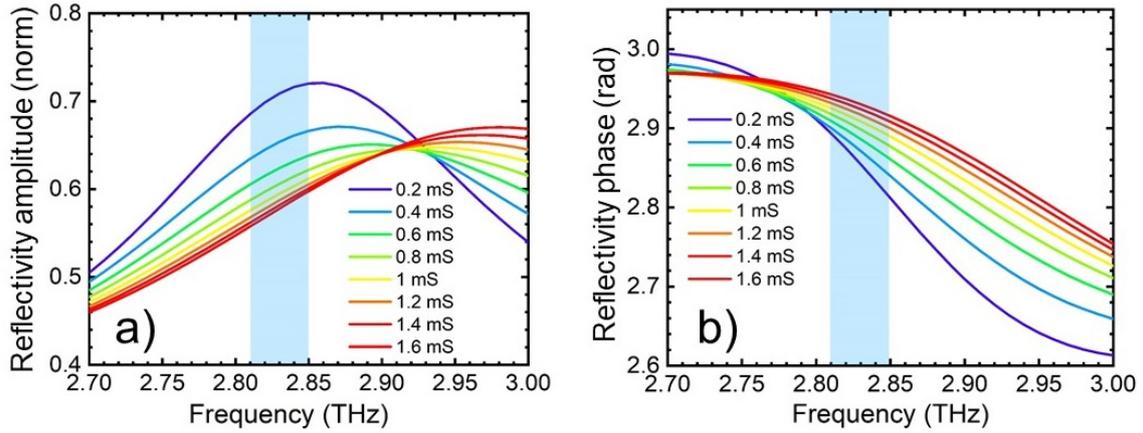

Figure 2: Absolute value a) and phase b) of the reflectivity of the EIT mirror for different graphene conductivities. The frequency range of the QCL emission is shown in the light blue areas.

outer C-shaped feature (y-axis). The Drude model was used to describe the complex conductivity of the graphene and the gold. Further information on the model used, including the fabrication parameters, are reported in [26, 27]. The simulated results for the complex reflectivity of the EIT mirror calculated at different graphene conductivity values are shown in Figure 2. The graphene conductivity range chosen between 0.2 mS and 1.6 mS is commensurate with the values retrieved from the DC measurements. Due to the relatively high resonant frequency and the limited bandwidth of the THz time domain spectrometer available, transmission measurements could not be performed for this sample. However, the excellent agreement between the FEM simulations, the theoretical circuital model and the measurements acquired for similar devices resonating at lower frequencies reinforce the validity of the numerical calculations. The EIT device was engineered in order to exhibit a dispersive trend in the reflectivity around 2.8-2.9 THz. The absolute value of the reflectivity peaks at 0.72 around 2.85 THz for 0.2 mS and decreases to ~ 0.58 for 1.6 mS. A maximum dynamic range of ~0.12 rad was achieved around 2.85 THz for the argument of the reflectivity in the considered conductivity range. The multi-mode reduced rate equations (1)-(4) (RREs) with optical feedback terms were used to simulate the EC-QCL mode competition and investigate the complex laser dynamics under different feedback conditions:

$$\frac{dN_3(t)}{dt} = \frac{\eta_3 I}{q} - \sum_m G_m \left(N_3(t) - N_2(t)\right)S_m(t) - \frac{N_3(t)}{\tau_3}, \tag{1}$$

$$\frac{dN_2(t)}{dt} = \frac{\eta_2 I}{q} + \sum_m G_m \left(N_3(t) - N_2(t)\right)S_m(t) + \frac{N_3(t)}{\tau_{32}} + \frac{N_3(t)}{\tau_{sp}} - \frac{N_2(t)}{\tau_2}, \tag{2}$$

$$\frac{dS_m(t)}{dt} = MG_m(N_3(t) - N_2(t))S_m(t) + \frac{M\beta_{sp}N_3(t)}{\tau_{sp}} - \frac{S_m(t)}{\tau_p} + \frac{2K_m}{\tau_{in}}\left(S_m(t)S_m(t - \tau_{ext})\right)^{\frac{1}{2}}\cos(\omega_{th}\tau_{ext} +$$

$$\varphi_m(t) - \varphi_m(t - \tau_{ext}) - ps_m), \tag{3}$$

$$\frac{d\varphi_m(t)}{dt} = \frac{\alpha}{2}\left(MG_m(N_3(t) - N_2(t)) - \frac{1}{\tau_{p,m}}\right) - \frac{K_m}{\tau_{in}}\left(\frac{S_m(t - \tau_{ext})}{S_m(t)}\right)^{\frac{1}{2}}\sin\left(\omega_{th,m}\tau_{ext} + \varphi_m(t) - \varphi_m(t - \tau_{ext}) -$$

$$ps_m). \tag{4}$$

Where $N_3(t)$ is the upper level electron population, $N_2(t)$ the lower level electron population, $S_m(t)$ the photon population at mode m, $\varphi_m(t)$ the phase of the electrical field at mode m, I the current flowing in the active region, q the electronic charge, respectively. Other parameters are described in Table 1.The QCL's transport parameters τ_3, τ_{32}, τ_2, η_3, η_2, G_p used in RREs have been calculated by the full self-consistent energy-balance Schrödinger–Poisson scattering transport calculation solver applied to this particular BTC THz QCL design [36]. The factor K_m is the feedback coupling coefficient for the mode m and is given by [37]:

$$K_m = \varepsilon \cdot (1 - R_2) \cdot \sqrt{\frac{R_m}{R_2}} \tag{5}$$

The optical feedback coefficient ε which takes into account the mode mismatch and other losses in the optical path, was left as a free fitting parameter. R_2=0.02 is the coated laser facet reflectivity, while R_m is the reflectivity of the target at the mode m frequency. The values of R_m and of the phase shift at mode m, ps_m, for the EIT mirror can be obtained from the FEM simulations and shown in Figure 2. When inserting the Au mirror, the values R_m =0.997 and ps_m =0 were used for all the modes in the simulation.

Table 1: parameters used in the RREs simulations and their values/definitions

Symbol	Description	Value/definition
τ_3	Total carrier lifetime in the upper laser level	5.0×10^{-12} s
τ_{32}	Non-radiative relaxation time from upper to lower lasing level	1.76×10^{-10} s

τ_2	Total carrier lifetime in the lower laser level	2.1×10^{-11} s
τ_{sp}	Spontaneous emission lifetime	1.0×10^{-6} s
$\tau_{p,\,m}$	Photon lifetime for mode m	6.32×10^{-12} s
τ_{ext}	External cavity round trip time	9.34×10^{-10} s
τ_{in}	Laser internal round trip time	$\tau_{in} = 2L_{in}/v_g$
β_{sp}	Spontaneous emission factor	1.627×10^{-4}
v_g	Group velocity	c/n$_g$
n_g	Laser cavity group refractive index	3.62
η_3	Injection efficiency into the upper lasing level	0.5441
η_2	Injection efficiency into the lower lasing level	0.0165
M	Number of periods in the active region	90
G_m	Gain factor of mode m, Lorentzian shape	$G_m = G_p \Big/ \left[\left(1 + \left(\frac{v_p - v_m}{\Delta v/2}\right)^2\right)\left(1 + \varepsilon_g S_m(t)\right)\right]$
G_p	Peak gain factor per period	1.8×10^{-4} s^{-1}/90
Δv	FWHM gain bandwidth	200 GHz
v_m	Frequency of mode m	Varies
v_p	Peak gain frequency	2.84 THz
ε_g	Gain compression coefficient	3.67×10^{-5}
ω_{th}	Laser mode angular frequency in the absence of optical feedback at threshold	$\omega_{th} = {m\pi c}\big/{n_{th} L_{in}}$
L_{in}	Laser cavity length (internal)	2.5 mm
α	Linewidth enhancement factor	-0.1 [28, 32]

In the simulations 7 modes, spaced by the free spectral range (FSR) of c/2$n_g L_{in}$=16.6 GHz centered around 2.84 THz were considered, assuming a FWHM bandwidth of 200 GHz. The mode frequencies are 2.781 THz, 2.798 THz, 2.814 THz, 2.831 THz, 2.847 THz, 2.864 THz,
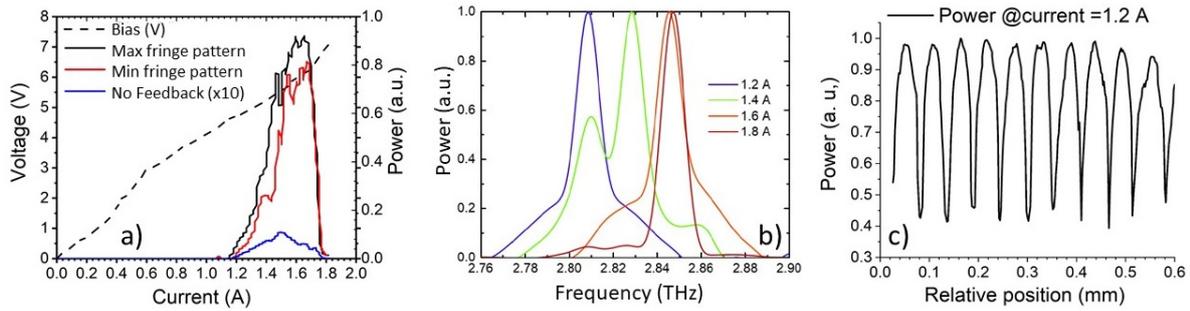
Figure 3: Au mirror EC-QCL measurements. a) VIL of the QCL recorded at a maximum of the interference pattern (black trace), together with the LI at a minimum (red line) and without feedback (blue line). b) Spectra of the EC-QCL with the Au mirror positioned at a maximum of the interference pattern. c) Interference fringes when sweeping the Au mirror close to threshold.

and 2.880 THz for the free-running laser with no optical feedback. Nevertheless, because of the partial lasing suppression and the limited capabilities of the FTIR available only the modes at frequencies of 2.814 THz, 2.831 THz, 2.847 THz were observed experimentally and investigated in detail, and are hereafter described as modes m 1-3 respectively.

In the first set of experiments, the Au mirror was positioned to form an external cavity length of ~ 14 cm. The power output of the EC-QCL was recorded as the Au mirror was translated along the cavity axis using a sub-micrometer precision motorized stage recording the interference fringes. The voltage–current-power (VIL) relationship of the EC-QCL recorded with the mirror positioned at the top of a fringe, together with the LIs acquired at a bottom of a fringe and without feedback are shown in Figure 3 a). Figure 3 b) presents the normalized
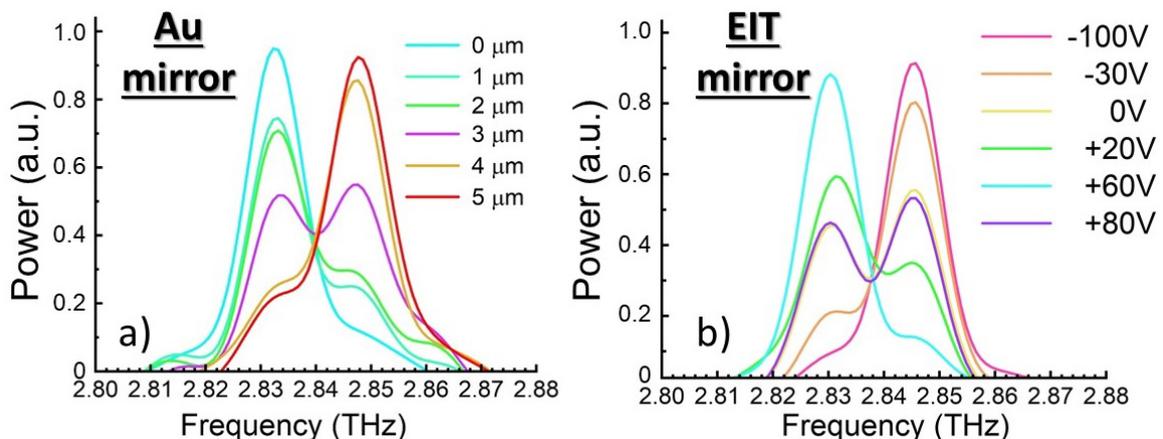

Figure 4: mode competition with the QCL driven at J_{max} a) by moving, with a micrometer stage, the Au mirror relative position around an external cavity distance of ~ 14 cm; b) by substituting the Au mirror with the EIT one, and performing a gate voltage sweep.

spectral content of the EC-QCL emission recorded with the Au mirror positioned at a top of a fringe for different QCL operating drive currents. Three lasing modes were emitted, with the

dominant mode hopping between approximately 2.81 THz and 2.85 THz as the current was increased in the range 1.2 A to 1.8 A. Finally, Figure 3 c) shows a typical fringe pattern recorded by sweeping the Au mirror position and keeping the QCL current at approximately 1.2 A, close to threshold, which yields more than 50% modulation of the emitted power.

In order to gain insight into the mode competition behavior of the complex EC-QCL system the mode switch between ~ 2.83 THz (mode 2) and ~ 2.85 THz (mode 3), shown in Figure 3 b) at I_{max} (~1.6 A) was investigated. Figure 4 a) shows the spectral content of the EC-QCL emission
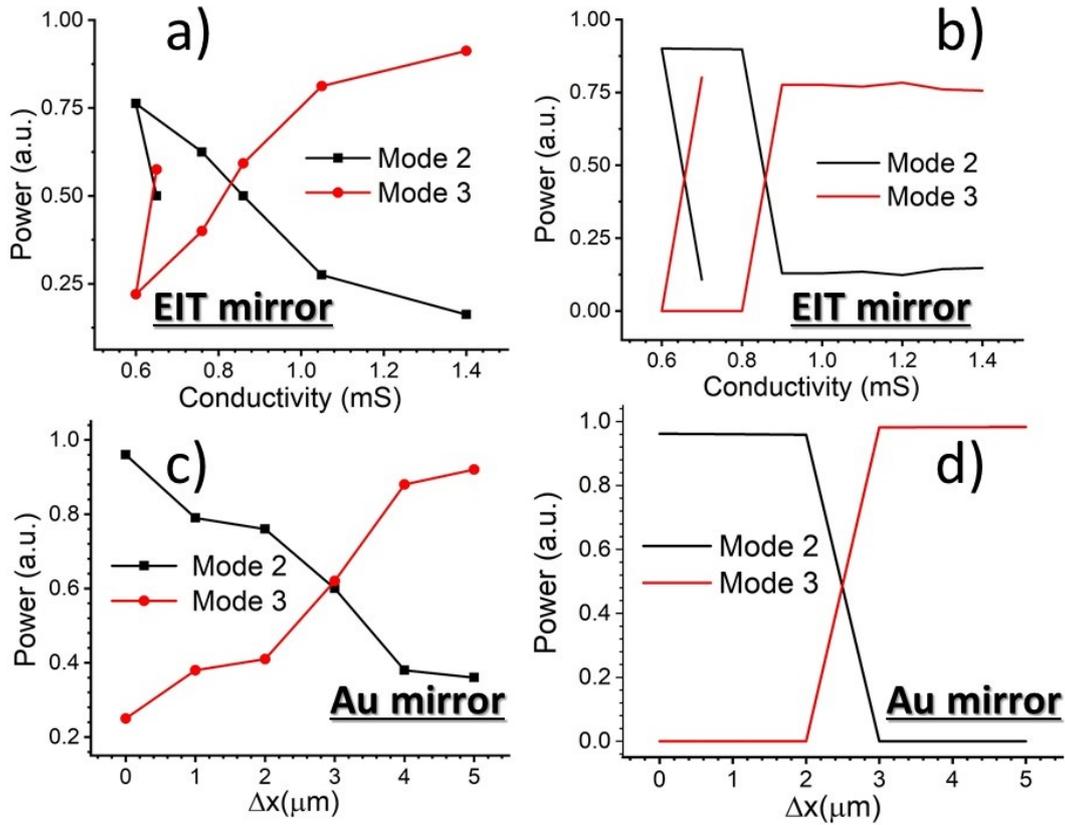
Figure 5. Power distribution for the mode switch between lasing mode 2 and 3. The EIT mirror experimental data and simulated curves with the RREs are showed in a) and b), respectively. The corresponding measured and theoretical prediction for the Au mirror are showed in c) and d).

acquired by keeping the laser current fixed at I_{max} and by increasing the external cavity length with the micrometer stage. The spectral power density is observed to shift to the higher-frequency mode as a result of the increasing round-trip phase of each mode. The mode switching behavior is nicely reproduced by using the EIT mirror at a fixed position and by performing a sweep of the graphene conductivity, as presented in Figure 4 b). In this case, the change in graphene conductivity modifies the complex refractive index and hence the

reflectance of the external EIT mirror, according to the simulations presented in Figure 2. It is interesting to highlight the switch from the 2.85 THz to the 2.83 THz mode which is completed at +60 V, corresponding to the charge neutrality point, and then reverses again at +80 V, corresponding to a relative increase in conductivity, as expected. This mode competition has been studied using the RREs frame described previously and the results are presented in Figure 5. Figure 5 a) shows the experimental data taken with the bolometer/FTIR, while Figure 5 b) shows the simulated results of the power switch between mode 2 and 3 with the EIT device as the feedback element. The model could correctly reproduce the turning point around 0.8 mS and the complete power redistribution from mode 3 to mode 2 at 0.6 mS. The mode power distribution has a non-univocal correspondence with the conductivity, as expected and reproduced by the model, since in the moderate to high feedback level the laser regime exhibits path hysteresis depending on the change of ε or φ_m [37]. The corresponding values for the optical feedback coefficient ε was 0.04172, yielding an Acket's [38] feedback parameter $C = K_m \frac{\tau_{ext}}{\tau_{in}} \sqrt{1 + \alpha^2}$ = 2.4~2.6. The experimental results and corresponding simulated curves for the mode switch achieved by axially translating the Au mirror are reported in Figures 5 c) and d), respectively, showing again a remarkable agreement. Assuming the same optical feedback coefficient for both feedback elements, the corresponding C parameter obtained for the Au reflective target measurements was ~ 4.5, corresponding to a moderate to strong feedback regime [35]. As expected, this value is larger than that determined for the EIT device as the Au has a higher reflectivity. The multi-mode THz QCL was operating in a tunable-mode regime when C > 1.83 with gain bandwidth of 200 GHz, where the mode competition is enhanced and the laser becomes very sensitive to the EIT tunable reflectance, as reported in [33].

In conclusion, the equivalence between THz EC-QCLs based on external reflective moving elements, such as an Au mirror, and a metamaterial/graphene optoelectronic mirror, whose reflectance can be tuned electronically, has been demonstrated in proof-of-principle experiments. The mode competition in the complex EC-QCL arrangements was described in the theoretical frame of RREs, confirming that the experimental configuration is consistent with the tunable mode regime. These results pave the way for the introduction of external, fast

reconfigurable all-electronic control of QCL emission for applications in spectroscopy and imaging, and at the same time provide a valuable tool for the theoretical investigation of the complex laser dynamics and mode competition in THz QCLs.

Data availability: the data that support the findings of this study are openly available from Lancaster University's repository at https://dx.doi.org/10.17635/lancaster/researchdata/371.

References

[1] L. H Li L. Chen, J.R. Freeman, M. Salih, P. Dean, A.G. Davies and E.H. Linfield Electron. Lett **53**(12), 799 (2017).

[2] L. Bosco, M Franckie, G. Scalari, M. Beck, A. Wacker, J. Faist, Appl. Phys. Lett. **115**, 010601 (2019).

[3] V Spagnolo, A. A. Kosterev, L. Dong, R. Lewicki, F. K. Tittel Appl. Phys. B **100**(1), 125, (2010)

[4] L. Consolino, S. Bartalini, H. E. Beere, D. A. Ritchie, M. S. Vitiello, P. De Natale Sensors, **13**(3), 3331(2013)

[5] Y. Ren, R. Wallis, D. S. Jessop, R. Degl'Innocenti, A. Klimont, H. E Beere, D. A Ritchie, App. Phys. Lett. **107**(1) 011107 (2015)

[6] P. Dean, Y. L. Lim, A. Valavanis, R. Kliese, M. Nikolić, S. P. Khanna, M. Lachab, D. Indjin, Z. Ikonić, P. Harrison, A. D. Rakić, E. H. Linfield, A. G. Davies Opt. Lett. **36**(13) 2587, (2011).

[7] A. D. Rakić, T. Taimre, K. Bertling, Y. L. Lim, P. Dean, A. Valavanis and D. Indjin, Appl. Phys. Rev. **6**, 021320 (2019).

[8] T. Nagatsuma, G. Ducournau and C. C. Renaud, Nat. Photon. **10**, 371 (2016)

[9] Y. Zeng, B. Qiang, Q. J. Wang, Adv. Optical Mater. 8, 1900573, (2020)

[10] J. Xu, d. B. Fenner, R. P. Green, L. Mahler, A. Tredicucci, M. G. Allen, F. Beltram, H. E. Beere, D. A. Ritchie Appl. Phys. Lett. **91**, 121104 (2007)

[11] Q. Qin, B. S. Williams, S. Kumar, J. L. Reno, Q. Hu, Nat. Photon.**3**, 732 (2009)

[12] I Kundu, J. R. Freeman, P. Dean, L. Li, E. H. Linfield, A. G. Davies ACS Photon. **7**, 765 (2020)

[13] I. Kundu, J. R. Freeman, P. Dean, L. H. Li,1 E. H. Linfield, A. G. Davies Opt. Express **28**(4), 4374 (2020)

[14] G. Liang, Y. Zeng, X. Hu, H. Yu, H. Liang, Y. Zhang, L. Li, A. G. Davies, E. H. Linfield Q. J. Wang. ACS Photon. 4, 517 (2017).

[15] C. A. Curwen, J. L. Reno and B. S. Williams, Appl. Phys. Lett. **113**, 011104 (2018)

[16] L. Xu, D. Chen, T. Itoh, J. L. Reno, B. S. Williams, Opt Express **24**(21) 24117 (2016)

[17] M. S. Vitiello, A. Tredicucci, IEEE Trans Terahertz Sci Technol, **1**(1), 76 (2011)

[18] C. A. Curwen, J. L. Reno, B. S. Williams, Nat. Photon. **13**, 855, (2019)

[19] F. Castellano, V. Bianchi, L. Li, J. Zhu, A. Tredicucci, E. H. Linfield, A. Giles Davies, M. S. Vitiello, Appl. Phys. Lett. **107**, 261108 (2015)

[20] I. Kundu, P. Dean, A. Valavanis, L. Chen, L. H. Li, J. E. Cunningham, E. H. Linfield, and A. G. Davies, Opt. Express **25**, 486 (2017)

[21] N. Han, A. de Geofroy, D. P. Burghoff, C. W. I. Chan, A. W. M. Lee, J. L. Reno, and Q. Hu, Opt. Lett. **39**, 3480 (2014)

[22] H. T. Chen, A. J. Taylor, N. Yu Rep. Prog. Phys. **79**, 076401 (2016)

[23] S. Lee, S. Baek, T.-T. Kim, H. Cho, S. Lee, S, Kang J-H, Min B Adv. Mater. 2000250 (2020)

[24] P. Q. Liu, I. J. Luxmoore, S. A. Mikhailov, N. A. Savostianova, F. Valmorra, J. Faist, G. R. Nash. Nat. Commun. **6**, 8969 (2015)

[25] Y. Sun, R. Degl'Innocenti, D. A. Ritchie, H. E. Beere, L. Xiao, M. Ruggiero, J. A. Zeitler, R. I. Stantchev, D. Chen, Z. Peng, E. MacPherson, and X. Liu Photon. Res. **6**, 1151 (2018)

[26] S. J. Kindness, N. W. Almond, B. Wei, R. Wallis, W. Michailow, V. S. Kamboj, P. Braeuninger-Weimer, S. Hofmann, H. E. Beere, D. A. Ritchie, R. Degl'Innocenti Adv. Optical Mater. **6** 1800570 (2018)

[27] S. J. Kindness, N. W. Almond, W. Michailow, B. Wei, L. A. Jakob, K. Delfanazari, P. Braeuninger-Weimer, S. Hofmann, H. E. Beere, D. A. Ritchie, R. Degl'Innocenti ACS Photonics **6**, 1547 (2019).

[28] T.-T. Kim, S. S. Oh, H.-D. Kim, H. S. Park, O. Hess, B. Min, S. Zhang Sci. Adv. **3**, e1701377 (2017)

[29] S. J. Kindness, D. S. Jessop, B. Wei, R. Wallis, V. S. Kamboj, L. Xiao, Y. Ren, P. Braeuninger-Weimer, A. I. Aria, S. Hofmann, H. E. Beere, D. A. Ritchie, R. Degl'Innocenti Sci. Rep. **7**(1), 1 (2017).

[30] Y. Ren, R. Wallis, Y. D. Shah, D. S. Jessop, R. Degl'Innocenti, A. Klimont, V. Kamboj, H. E. Beere, D. A. Ritchie Appl. Phys. Lett. **105**(14), 141102, (2014)

[31] B. Wei, S. J. Kindness, N. W. Almond, R. Wallis, Y. Wu, Y. Ren, S. C. Shi, P. Braeuninger-Weimer, S. Hofmann, H. E. Beere, D. A. Ritchie, R. Degl'Innocenti Appl. Phys. Lett. **112**(20) 201102 (2018).

[32] X. Qi, G. Agnew, I. Kundu, T. Taimre, Y. L. Lim, K. Bertling, P. Dean, A. Grier, A. Valavanis, and E. H. Linfield, A. G. Davies, D. Indjin, and A. D. Rakić, Opt. Express **25**(9), 10153 (2017)

[33] X. Qi, G. Agnew, T. Taimre, S. Han, Y. L. Lim, K. Bertling, A. Demić, P. Dean, D. Indjin, A. Rakić; Opt. Express 28(10), 14246 (2020)

[34] F. Wang, V. Pistore, M. Riesch, H. Nong, P.-B. Vigneron, R. Colombelli, O. Parillaud, J. Mangeney, J. Tignon, C. Jirauschek and S. S. Dhillon Light: Science & Applications, **9**, 51 (2020)

[35] P. Braeuninger-Weimer, B. Brennan, A. J. Pollard, S. Hofmann Chem. Mater. 28(24), 8905

(2016)

[36] G. Agnew, A. Grier, T. Taimre, Y. L. Lim, M. Nikolić, A. Valavanis, J. Cooper, P. Dean, S. P. Khanna, M. Lachab, E. H. Linfield, A. G. Davies, P. Harrison, Z. Ikonić, D. Indjin, A. D. Rakić, Appl. Phys. Lett. **106**, 161105 (2015)

[37] T. Taimre, M. Nikolic, K. Bertling, Y. L. Lim, T. Bosch, A. D. Rakić, Adv. Opt. Photonics, **7**(3), 570 (2015)

[38] G. A. Acket, D. Lenstra, J. den Boef, B. H. Verbeek, IEEE J. Quantum Electron. **20**, 1163 (1984).